HARVARD UNIVERSITY

HARVARD COLLEGE OBSERVATORY

SEMIANNUAL STATUS REPORTS NOS. 9 AND 10

July 1, 1974 through June 30, 1975

NASA Grant NGR 22-007-202

Rocket Spectrometer for Investigation of the Far Ultraviolet Solar Spectrum

Principal Investigator: W. H. Parkinson
Co-Investigator: E. M. Reeves
Co-Investigator: J. L. Kohl

I. Introduction

On September 18, 1974 we accomplished the 6th and final flight of our rocket-borne Ebert spectrometer and telescope. For this flight the instrument was arranged in the high resolution line scanning mode with 0.03 Å spectral resolution. We scanned selected emission lines between 1,170 and 1,640 Å with the high resolution and also made a complete wavelength scan from 1170 Å to 1850 Å with 5 Å resolution. We were able to make accurate measurements of the line profiles of the He II lines at 1640 Å, C IV lines at 1550 Å, Si IV lines at 1400 Å, C II lines at 1335 Å, the N V lines at 1240 Å, and the C III lines at 1175 Å.

Information about each of our rocket flights is outlined in Table I. We have accurate intensity measurements of the quiet sun spectrum for wavelengths between 1174 Å and 3220 Å. The spectral resolution (defined by the full width at half maximum of the instrumental profile) is better than 0.03 Å over most of the range and the spatial resolution is relatively low so that the observations are averaged over the chromospheric network.

During the past grant year we concentrated on the reduction and analysis of these data with two aims in mind: 1) We prepared plots of absolute intensity versus wavelength for the full wavelength range of our observations so that the spectra can be published in the form of a solar atlas to be published as a NASA special report or similar U.S. Government document, 2) We

prepared and presented papers at scientific meetings and prepared papers for publication that describe the relationship of our data to some of the important problems in solar physics.

J.L. Kohl (1974) described our observations of the center and limb spectra of the wavelength range between 2250 Å and 3220 Å at IAU Colloquium No. 27 which was held here at Harvard in September 1974. Many of the solar and stellar astrophysicists attending the Colloquium expressed a definite interest in the data. We believe that our data is the most complete set of absolute intensity measurements at high spectral resolution that exist for this wavelength range of the solar spectrum.

J.L. Kohl (Kohl, Parkinson, and Reeves, 1975) presented the observations of our most recent rocket flight at the meeting of the solar division of the AAS that was held at the University of Colorado in January 1975. An interesting discussion followed the presentation. This included discussions of a possible emission center of the Mg I λ2852 line, the absolute spectral radiance for wavelengths between 1400 and 1850 Å, and the implications of apparent nonthermal velocity components of lines formed in the chromosphere-corona transition region.

We have submitted an abstract for the 146th Meeting of the American Astronomical Society (J.L. Kohl and W.H. Parkinson, 1975). The paper is entitled "The Solar Profiles of the Components of He II 1640 Å from rocket observations".

We have completed our work with the Mg II h and k lines and have prepared a paper for publication entitled "The Magnesium II h and k Lines I: Absolute Center and Limb Measurements of the Solar Profiles" (J.L. Kohl and W.H. Parkinson, 1975b). Paper 2, by T.R. Ayres and J.L. Linsky of JILA is entitled "The Magnesium II h and k Lines II: Comparison with Synthesized Profiles and Calcium IIK". The two papers will be prepared as a Center for Astrophysics preprint.

During the past grant year we prepared magnetic tapes of the data in the 1174 Å to 2400 Å range for the OSO I experimenters. The recorded information gave the absolute spectral radiance of the quiet sun spectrum as a function of wavelength with .02 Å wavelength steps. The data were supplied to help prepare the OSO I observing programs and to determine the OSO I instrument requirements (spatial and spectral resolution, and integration time).

This grant also supported the experiment definition and design studies of the Ly α coronagraph system and the measurements of the scattered light properties of a simulated Ly α instrument.

II. Scientific Program

II-1. Measurements of the Mg II h and k solar profiles

We have prepared a paper for publication that describes our measurements of solar Mg II h and k profiles. The uncertainties in the absolute intensities at k_1 and h_1 are -20 to +12 percent with smaller uncertainties for higher intensities. The spectral resolution, defined by the FWHM of the instrumental profile, was 0.028 Å and the angular resolution element was 184" by 1.5". Measurements were made for a quiet region near the disk center and for a quiet region at cos Θ = 0.23. The measured profiles are suitable for detailed comparisons with theoretical solar and stellar profiles. Our measured minimum intensities (k_1 and h_1) relative to the core intensities (k_3 and h_3) and to the average peak intensities (k_2 and h_2) are fainter than the corresponding intensities that were reported by Lemaire and Skumanich (1973). In paper II, Ayres and Linsky find that the HSRA and VAL models (Vernazza, Avrett and Loeser, 1973) predict systematically lower intensities in the Mg h and k, and the Ca II K inner wings than we measured, but that a model with a somewhat higher temperature minimum can reproduce the measured inner wing intensities and limb darkening of these resonance lines. In addition, they find that the HSRA and VAL models predict systematically lower emission intensities than observed in the Ca II K and Mg II h and k cores. This disagreement suggests that both models are too cool in the regions of the low chromosphere where the k and K source functions

peak. They therefore propose a hot temperature minimum solar model which is reasonably consistent with our measured emission cores and wing intensities of Mg II and also consistent with the Ca II observations.

An overall view of our measurements of Mg II h and k, for observations at sun center and near the solar limb, is shown in Figure 1. The ordinates represent the spectral intensities on an absolute scale that we believe is accurate to better than $\pm$ 12 percent. The wavelength scale is based on the laboratory wavelengths (in air) of lines identified in the wings of Mg II h and k and at shorter and longer wavelengths. The wavelength scale was not corrected for the solar wavelength shifts.

The intensity structure in Figure 1 is due to the solar spectrum, not to statistical fluctuations, which have about a 5 percent standard deviation for observations of the line wings. The observations were subject to an occasional electronic noise burst that appeared as an increase in intensity and, less often, there were short interruptions (1 - 5 ms) of the signal. These sections of the data could be identified because they were not consistent for the two scans of the spectrum at the center or at the near limb pointing coordinates.

We could almost always determine which scan was in error by examining the data after they had been filtered by Fourier transform techniques. We found that the power spectrum of the

noise bursts and signal interruptions contained large high-frequency components that, when filtered out of the data, tended to move the smoothed points outside the statistical error bars of the noisy data and toward the correct values. A few such areas were removed from Figure 1.

b) Background Noise

A definitive measurement of the intensity of Mg II h and k that includes the absolute values of the h_1 and k_1 minima must take account of the instrumental background level that should be accurately known. One source of background noise that is completely negligible in our case is the continuous electronic and photomultiplier noise (about 0.006 counts are accumulated during the time to scan 0.01 Å). The noise bursts discussed in above are not a problem since they do not repeat from scan to scan.

Instrumental scattered light can be a serious problem for measurements of this kind but it was not a problem for this work. The amount of scattered light due to wavelengths well away from the wavelength of interest was determined from measurements made during the flight for center pointing and again for limb pointing. The measurements were made by quickly scanning the full wavelength range while an absorption filter covered the entrance slit. To reject lower wavelengths, a quartz window was always present between the exit slit and the detector. The scattered light for this flight was found to be independent of the wavelength setting

of the spectrometer and changed by only one percent between center and limb. We have attributed the measured scattered light level to light leaks near the detector.

Another source is scattering inside the spectrometer of light with wavelengths near the wavelength being scanned. We did not expect this to be a problem for this flight because the spectrometer, with the holographically produced grating, has an exceptionally low scattered-light level and no detectable ruling ghosts. The efficiency of the instrumental profile at 1.0 Å from line center is about 5×10^{-5} of the peak efficiency. As an upper limit, we have assumed that the efficiency remains at this level for $\pm$ 30 Å where the efficiency falls to zero. With this assumption, we estimate an uncertainty in the k_1 and h_1 minimum intensities of -8 to 0 percent due to scattered light. Further evidence for a low scattered-light level can be found from the observed minimum intensities of lines near Mg II h and k. For example, we have identified all three members of the Mn I (UV multiplet No. 1) lines at 2801.084 Å, 2798.270 Å, and 2794.817 Å in the solar spectrum. Two of the lines are indicated in Figure 2. The line at 2794.817 Å, which is located very near the k_{1v} minimum, has an intensity at line center that is well below the measured minima of h_1 and k_1.

c) The Mg II h and k Centers

Our observations of the emission centers of Mg II h and k are shown in Figure 2. The data points are the raw data intensities

for 0.01 Å intervals. For convenience, every third data point has been plotted. Triangles and crosses represent the individual scans and the solid lines represent the average intensities of two scans that have been smoothed with a gaussian filter with a full width of 0.02 Å. A few points that have been identified as noise were removed from the data before the final filtering operation. Noise was not removed from the raw data points of Figure 2. The values of the smoothed average intensities are given in Table 2.

Since we have used a scanning spectrometer, the statistical fluctuations of the data depend on the wavelength interval for each data point. The error bars for the raw data (shown in Fig. 2) represent one standard deviation for wavelength intervals of 0.01 Å. The Fourier filtering process used to produce the solid line curve in Figure 2 reduces the statistical uncertainty, as would an increase in the data point wavelength interval.

d) The Features of the Profiles

In order to facilitate comparisons of our measurements with other experimental data and with theoretical models (see paper II), we have used the data in Table 2 to determine the wavelengths and spectral intensities of the inflection points in the Mg II h and k profil s. These results are given in Table 3. Because of the presence of the Mn I line (2794.817 Å) near k_{1v}, the information for k_{1v} is ambiguous and was omitted therefore from Table 3. For $\mu = 1$, our measured wavelength separations relative

to line center "$\Delta\lambda$" of the h_1 and k_1 minima are slightly larger than the values determined by Milkey and Mihalas (1974) from the measurements of Lemaire (1971). Our corresponding $\Delta\lambda$'s for the profiles at $\mu = 0.23$ are larger than our values of $\Delta\lambda$ for the center profiles.

In Table 4, we compare our relative intensities and wavelength separations to the "k reference profile" of Lemaire and Skumanich (1973). The agreement is good for the separation of the peaks and for the FWHM. Their value for the ratio of the mean peak intensity to the core intensity is outside our estimated error limit. The major differences in the two sets of measurements are the respective values for the ratio between the core intensity and the minimum intensity. Their value for k_1 lies well outside our error limits. Their corresponding ratio for h is 1.86 compared with our ratio of 3.59. The ratios between the averaged peak intensity and the minimum intensity for the k line at $\mu = 1$ are 6.36 for this work and 5.14 for Lemaire and Skumanich (1973). In Figure 3, we compare h to k for the center and for the near limb spectra. We have not considered the k_{1v} minimum in detail because of the ambiguity introduced by the Mn I line. We find: (1) h is more intense than k for any $\Delta\lambda$ beyond 0.50 Å for $\mu = 1$, and beyond 0.55 Å for $\mu = 0.23$; (2) h lies below k throughout the core for both $\mu = 1$ and 0.23; (3) the ratio of the k_3 and h_3 intensities is 1.14 and 1.21 for $\mu = 1$ and 0.23 respectively; (4) the absolute spectral intensities of

h_{1r} and k_{1r} are almost equal although h_{1r} appears to be slightly fainter than k_{1r} at the disk center and slightly stronger at $\mu = 0.23$.

We have attempted to determine the absolute intensity profiles that are representative of the Mg II h and k wings. This was done by selecting sections of the observed spectra that are apparently free of absorption lines. The results for $\mu = 1$ and 0.23 are given in Figure 4.

In Figure 5 we give the limb-to-center intensity ratio as a function of wavelength. The intensity values used for the wings are those plotted in Figure 4 and the values used for the center emission features are the intensities of the inflection points from Table 3.

II-2. The Solar Profiles of the Components of He II 1640 Å from Rocket Observations

We have made high spectral resolution measurements (0.03 Å) of the shape and absolute intensity of the solar emission feature at 1640 Å on July 27, 1972 and again on Sept. 18, 1974 (see figure 6). The measurements are of the average spectral intensity of rectangular regions (16 arc min by a few arc seconds) that are centered on the solar disk. A rocket-borne Ebert spectrometer with a photoelectric detector was used for the observations. Both sets of observations clearly separate the

Fe II line at 1640.150 Å from the He II line. We find that the intensity and half width of the Fe II line are the same for the two observations to within the experimental uncertainties. A component that is primarily (about 90 percent) He II $2p\ ^2P_{3/2}$-$3d\ ^2D_{5/2}$ at 1640.474 Å is clearly resolved from a blend of the $2p\ ^2P_{1/2}$-$3d\ ^2D_{3/2}$ and $2s\ ^2S$-$3p\ ^2P$ components centered at 1640.36 Å (see figure 7). It is also clear that the $2p\ ^2P_{3/2}$-$3s\ ^2S_{1/2}$ component at 1640.533 Å is very weak. Assuming that the relative intensities of transitions from a single fine structure level are proportional to the atomic line strengths and that all components have identical widths, we have subtracted the contribution of the $2p\ ^2P_{1/2}$-$3d\ ^2D_{3/2}$ transition from the 1640.36 Å blend and thus determined the line profiles for the $2s\ ^2S_{1/2}$-$3p\ ^2P$ transitions. In this way, we have determined the profiles of each of the components of the Hα line of He II. The absolute intensities of the components will be compared to the measurements of Timothy (1975) to determine the optical thickness and therefore the attenuation of the He II Ly β line at 256 Å. The widths of the components is an indication of the kinetic ion temperature in the region of formation of the He II Hα line. The results of this work are expected to provide new insight into the problem of the possible excitation mechanisms of He II and the understanding of the transition region.

This work will continue into the next report period and a paper for publication will be prepared.

II-3. The Solar Abundance of B I

The center and limb spectra of the sun obtained during our rocket flight of May 15, 1975 have revealed absorption features that correspond in wavelength to the BI resonance lines at λ(air) = 2497.7233 Å and 2496.7717 Å. J.L. Kohl, W.H. Parkinson and G. Withbroe are using these data and spectral synthesis methods to set limits on the solar BI abundance.

The solar boron abundance problem was recently discussed by N.B. Hall and O. Engvold (1975). They point out that there has been no positive detection of the element boron in the sun's surface layers. Their new abundance and the earlier abundance determination of N. Grevesse (1968) and H. Wohl (1974) have been derived, essentially, from the absence of infrared atomic lines from the photospheric spectrum.

The explanation of the abundance of boron in the stars, in the sun, and in meteorites is not yet satisfactory (C. Ryter, et. al. 1970; H. Reeves, et al., 1970; and A.G.W. Cameron, S.A. Colgate, and L. Grossman). The recent developments which are described in these works make it highly desirable to obtain a value for the solar boron abundance.

The method of spectral synthesis requires basic atomic data (wavelengths, excitation energies, gf-values) and solar data to fully describe the emergent intensity in the wavelength region of

the BI spectral lines. The atomic data are well determined for the BI lines themselves but the neighboring lines in the spectrum do not have well determined atomic parameters.

The soalr BI line at 2496.7717 Å is partially overlapped by a Co I line with a poorly known wavelength. Dr. F. Tomkins of Argonne National Laboratory at our request has now made measurements of the wavelength of the Co I line which he resolved into three hyperfine structure components with uncertainties of about ± .0005 Å. This precision is sufficient for our synthetic spectrum analysis.

Weak absorption lines of Cr I are present in the solar spectrum within ± 2 Å of the BI lines. These weak lines are expected to lie on the linear part of the solar curve of growth. Since the Cr abundance is reasonably well known, an analysis of the Cr I lines can be used to establish the solar continuum level in the region of the BI lines and can also be used as a general check on the validity of the synthesized spectrum. Fortunately, measurements of the log gf-values of the Cr I lines have just been completed in our laboratory (Huber, Sandeman and Tubbs, 1975).

II-4. Line Profiles of Lines Formed in the Transition Region

We have continued to reduce the data from our observations of C III λ 1176, C IV λ 1548, Si IV λ 1402, and N V λ 1238. We have made least squares fits of these lines to pure gaussian profiles

and determined the intensities and widths of each spectral line. We find that all of these lines have a non-thermal velocity component of 24 $\pm$ 1 km/sec. We have also measured the relative intensities of the individual members of each multiplet. The relative intensities within the C III multiplet are known to be electron density sensitive (Gabriel and Jordan, 1972). Our preliminary analysis of the lines indicate that the lines are fully mixed (i.e. have the relative intensities of the theoretical line strengths). This information can be used to establish a lower limit on the electron density at the region of formation of the lines. A more complete analysis of the transition region lines is planned for the next grant period.

II-5. Determination of the Absolute Spectral Intensity of the Quiet Sun

Using the data from all of our rocket flights, we have continued to improve the accuracy of our values for absolute spectral intensity of the sun. This requires a determination of linearity corrections, background intensities and noise, absorption by residual water vapor in the instrument during the data acquisition period, atmospheric absorption, and calibration uncertainties. Our absolute intensity measurements and analysis are approaching completion and we plan to publish the final results during the next grant period.

The intensity calibration at the wavelengths of Mg II h and k

was crucial to Dr. Ayres and Linskys' analysis. A description of that calibration follows.

a) Calibration Based on a Standard Photodiode

Although we measured the efficiency of most of the elements of the rocket instrument individually, the total spectrometer, telescope, and detection system were finally calibrated as a unit. This radiometric calibration was divided into two wavelength ranges. For the shorter wavelengths (2250 Å to 2528 Å) the calibration was based on Spicer diode Serial No. 127, a special photodiode that has a magnesium fluoride window and a cesium telluride cathode. This detector was calibrated at the U.S. National Bureau of Standards (NBS) by direct comparison of photocurrents with an NBS calibrated standard photodiode. Our method of calibration for the short wavelength range was almost identical to the methods we used for earlier flights and has been described fully (Kohl and Parkinson 1974).

b) Calibration Based on a Standard Lamp

For wavelengths between 2516 Å and 3200 Å, the radiometric calibration is based on the calibration of a Philips tungsten ribbon standard of spectral radiance. The lamp current was measured with a Weston model 1971 dc ammeter that

was calibrated before and immediately after the calibration of the rocket instrument. The brightness temperature of the lamp was determined originally by Philips Research Laboratories and then recalibrated at Eppley Laboratories and periodically at Harvard by a direct comparison with another Philips lamp that is used as a laboratory standard (Huber and Parkinson 1972). The values for the emissivity of tungsten that are also required were taken from De Vos (1954).

For this calibration, the telescope system was removed and a calibrated portion of the tungsten ribbon lamp was focused directly onto the spectrometer entrance slit. The solid angle was defined by a circular aperture that was placed against the focusing lens on the side nearest the standard lamp. The size of the aperture stop was set to just underfill the spectrometer grating. Smaller apertures were also used to check for spatial nonuniformities. The system calibration was found to be independent of the part of the optics used. Another consistency test was to use more than one lamp current for the calibration at a given wavelength. The calibration was found to be independent of the lamp current within 1 - 2 percent.

c) The System Calibration Function

The solar data are reduced by use of our basic calibration equation:

$$\int_{\lambda_1}^{\lambda_2} I_\odot(\lambda)d\lambda = S(\bar{\lambda}) \int_{\lambda_1}^{\lambda_2} \frac{K(\lambda', t)d\lambda'}{\Delta\lambda\Delta t} \Big/ R_t A_s \Omega_t$$

where $\int I(\lambda)d\lambda$ is the integrated intensity in photons $s^{-1}cm^{-2}sr^{-1}$ for any wavelength interval $\lambda_2 - \lambda_1$, R_t is the reflectance of the telescope objective, A_s is the area of the entrance slit, Ω_t is the solid angle subtended by the telescope at the entrance slit, $K(\lambda', t)$ is the number of detector counts accumulated in a time interval Δt during which the spectrometer scans a small wavelength interval centered at λ', and $\Delta\lambda$ is the bandpass of the spectrometer exit slit. The system function, $S(\lambda)$, is the response of the instrument and detection system in photons per detector count, and is left outside the integral for wavelength intervals over which the response can be considered constant. In practice, Δt is usually the time interval during which the wavelength interval $\lambda_2 - \lambda_1$ is scanned.

A plot of $S(\lambda)$ is given in Figure 3. The open circles are based on the NBS calibration of our Spicer diode and the

solid circles are based on the calibration of our Philips lamp. Near 2520 Å the calibration based on the standard detector can be compared with the calibration based on the standard light source. The agreement is excellent, 5.1 percent difference between the two types of calibrations. This agreement, although not at all obvious while the calibration data were being taken, was found immediately when the calibration data were being reduced. No corrections or modifications of the calibration arrangement or procedure needed to be made.

As pointed out earlier (Kohl and Parkinson 1974) one of the larger sources of error is the widths of the spectrometer slits. Therefore, we determined values of $S(\lambda)$ using the flight slits as well as wider slits that have more easily measured widths. The results agreed to within 3 percent.

III. The Scattered Light Properties of the Simulated Ly-α Instrument

The unique requirement for the Ly-α instrument is that the instrumentally scattered Ly-α radiation from the chromosphere must be reduced in magnitude to a level that is well below the coronal Ly-α light level. In this section, we describe laboratory tests that were conducted here to determine the feasibility of this requirement.

The purpose of the scattered light tests was to compare, under simulated observational conditions, the amount of instrument-scattered light that is detected by the Ly-α coronagraph-spectrometer and the expected amount of detectable coronal light. The test facility illustrated in Figure 8 consists of a "mock-up" of the envisioned coronagraph-spectrometer, a polychromatic solar simulator, and a Hunter discharge lamp that is the light source for the simulator. Because of the simplicity of the Kr spectrum (lack of lines in the EUV), it was convenient to use the Kr line at 1235 Å for the tests rather than Ly-α. The coronagraph-spectrometer is represented in the test arrangement in the following way: a single linear knife edge, O_1 that can be considered to be aligned parallel to a tangent of the solar disk, is placed in the vacuum tank and a 50 cm focal length telescope mirror, M_1 is placed 200 cm behind the knife edge. The telescope focuses the simulated observation point of the corona (just a point in

space) on a 0.03 cm diameter aperture that corresponds to the coronagraph-spectrometer entrance slit S_1 (henceforth called "slit"). A spherical mirror M_2, placed 50 cm beyond the side of the slit opposite the telescope mirror images the slit onto a calibrated EMR 641-G multiplier phototube D_1. Together, the slit, spherical mirror and detector represent the spectrometer section of the coronagraph-spectrometer. The telescope mirror, in addition to focussing the solar corona onto the entrance slit, forms an image of the knife edge occulter 17 cm beyond the slit inside the spectrometer section. The spectrometer entrance slit acts as an aperture stop for the light that is both scattered by the knife edge and focussed by the telescope mirror. Therefore, the bundle of rays passing through the slit and converging to the image of the knife edge, inside the spectrometer, has a very high f-number (greater than f/200). An internal occulter strip placed at this image would be expected to reduce greatly the amount of scattered light passing through the spectrometer. Since the f-number for scattered light from the knife edge is much larger than the f-number of the coronal light, the best position for the internal occulter strip is very near the spectrometer mirror (the telescope forms an image of the corona on the slit and the light diverges with the f-number of the illuminated portion of the telescope). The test arrangement includes an electric drive system that is used to insert, in vacuum, the internal occulter strip O_2 into the image of the knife edge or

into the divergent beam from that image. The same device can also be used to insert a large blocking mask O_3 into the beam for a test of the amount of background light. For some of the tests, the EMR 641-G detector was placed immediately behind the spectrmeter entrance slit, D_2.

The mock-up of the coronagraph spectrometer was built mostly from existing optics and other components that were available in our laboratory. The requirements for the solar simulator were more exacting and this necessitated the purchase of special optical components.

For the solar simulator to illuminate the knife edge as the sun would, the field angle of the collimated beam must be 32 minutes. In the direction perpendicular to the knife edge, the collimating mirror M_3 itself must subtend this same angle as seen by the knife edge so the telescope mirror will not see the collimating mirror directly. A further constraint of alignment tolerances dictated a moderately sized mirror which then had to be located several meters from the knife edge to fulfill the angular requirements. In order to illuminate the full length of the occulter, the rectangular collimating mirror subtended a considerably larger angle in the direction along the length of the occulter.

For the tests, the coronagraph telescope mirror was placed in several positions to image different areas in space onto the entrance slit. The areas correspond to small areas in the corona

(about 3 arc min in diameter) between 1.5 $R_\odot$ and 2.5 $R_\odot$. The tests consisted of first measuring the intensity of the light incident on the occulter with a calibrated tungsten diode probe D_3. This probe also interrupted all of the direct illumination of the knife edge occulter, and this provided a measure of the background light as seen by the coronagraph-spectrometer detector. When the tungsten diode was moved away from the light path, the coronagraph-spectrometer detector system would determine the amount of light scattered into the instrument for a known illumination of the knife edge. Since the number of photons per unit area illuminating the knife edge was known, we could determine the apparent solar spectral intensity of the simulator, and this could be used with theoretical Ly-α intensities of the solar corona to calculate the amount of Ly-α radiation that we would expect to detect during an actual observation. For the case where an internal occulter was not used, the expected coronal signal for an area at 2.0 $R_\odot$ was about a factor of two larger than the measured scattered light signal. The internal occulter strip improved the scattered light rejection by an additional factor of 25, so the expected signal to scattered light ratio is about 50 for observations at 2.0 $R_\odot$ and is also acceptable at 3 $R_\odot$. The scattered light rejection was equally good for both the case when the internal occulter strip was placed at the focus of the knife edge occulter and when it was near the spectrometer mirror.

For observations at 1.5 $R_\odot$ and larger, the internal occulter reduces the coronal light signal by less than ten percent and the scattered light by more than an order of magnitude. Finally, we should point out that the entrance slit dimensions of the envisioned high dispersion spectrometer are large, compared to 1216 Å, so that diffraction from the slit is not a problem.

The tests have proven the feasibility of building a Ly-α coronagraph-spectrometer that will depend on a single linear occulting knife edge and an internal occulting strip for reducing the amount of scattered light to an acceptable level. A flight instrument with a scattered light rejection similar to the test instrument would have an instrumental scattered light background signal at Ly-α that would be well below the singal levels from the coronal Ly-α radiation for observations out to 3 $R_\odot$. We expect that the instrumental scattered light characteristics of the flight instrument will be acceptable for observations out to 4 $R_\odot$. Additional scattered light rejection could be achieved by employing three external occulters in an apodizing arrangement (MacQueen, 1968).

TABLE I

Name and Date	Wavelength Range (Å)	Spectral Resolution (Å)	Spatial Resolution (slit dimensions in equivalent arc min	Pointing Coordinates	Comments
NASA 4.185 US Sept. 24, 1968	1400-1875	0.06	16 by less than one	Random	Pointing contr failed. Measured EUV average intensities.
NASA 4.193 US Sept. 11, 1969	1300-1850	0.058	16 by less than one	Centered on the solar disk	Fully successful
NASA 13:031 US July 27, 1972	1547-1660	0.028	16 by less than one	Centered on the solar disk	Successful but only 1.3 scans because nose cone ejected late
NASA 13:032 US March 5, 1973	1830-2260	0.058	12 by less than one	Centered on the solar disk	Fully successful
NASA 26:018 US May 15, 1974	2250-3220	0.026	3 by less than one	Centered on the solar disk and about one arc min inside the east limb	Fully successful
NASA 13:035 US Sept. 18, 1974	1174-1850	0.030	16 by less than one	Centered on the solar disk	Fully successful
NASA 4.137 US March 7, 1970	850-2150	.05-.03	.27 no slit	Wide field excellent pointing stability	Successful

TABLE 1

Absolute Spectral Intensities of MgII h and k

λ_{air} (Å)	$I(\lambda)\times10^{-12}$ ■ $\mu=1$	$I(\lambda)\times10^{-12}$ $\mu=0230$	λ_{air} (Å)	$I(\lambda)\times10^{-12}$ ■ $\mu=1$	$I(\lambda)\times10^{-12}$ $\mu=0230$	λ_{air} (Å)	$I(\lambda)\times10^{-12}$ ■ $\mu=1$	$I(\lambda)\times10^{-12}$ $\mu=0230$	λ_{air} (Å)	$I(\lambda)\times10^{-12}$ ■ $\mu=1$	$I(\lambda)\times10^{-12}$ $\mu=0230$
2793.46	13.32	8.41	2794.34	9.90	6.49	2795.23	18.97	10.44	2796.11	6.25	3.61
2793.47	13.08	8.41	2794.35	10.42	5.85	2795.24	21.76	10.67	2796.12	5.18	3.71
2793.48	13.22	8.18	2794.37	9.71	5.60	2795.25	23.80	22.14	2796.13	4.97	5.07
2793.49	13.68	9.24	2794.38	9.39	6.15	2795.26	24.14	24.3	2796.15	4.83	5.61
2793.50	13.83	9.19	2794.39	10.52	6.84	2795.27	29.97	27.34	2796.16	4.59	4.08
2793.52	13.31	7.83	2794.40	11.25	5.80	2795.28	33.30	31.52	2796.17	4.66	3.69
2793.53	14.55	6.53	2794.41	9.92	4.45	2795.29	35.02	33.93	2796.18	5.75	2.82
2793.54	14.92	6.49	2794.42	7.78	4.00	2795.31	36.04	35.55	2796.19	6.70	3.59
2793.55	13.61	8.19	2794.43	7.55	4.76	2795.32	36.16	37.91	2796.20	6.33	4.37
2793.56	13.53	6.54	2794.44	6.28	5.17	2795.33	41.07	38.09	2796.21	6.61	4.54
2793.57	14.25	6.31	2794.46	9.11	5.55	2795.34	43.77	39.27	2796.22	6.09	3.67
2793.58	13.92	6.97	2794.47	9.25	5.59	2795.35	45.8	38.87	2796.23	6.28	3.91
2793.59	12.07	7.54	2794.48	8.25	5.46	2795.36	47.	38.71	2796.25	6.61	3.65
2793.60	11.14	8.51	2794.49	7.82	5.24	2795.37	50.	39.68	2796.26	6.14	4.44
2793.62	11.14	8.76	2794.50	7.72	4.04	2795.38	51.43	29.67	2796.27	5.91	5.04
2793.63	10.44	9.07	2794.51	8.97	3.17	2795.40	48.25	25.60	2796.28	6.37	4.26
2793.64	10.35	8.63	2794.52	9.21	3.50	2795.41	40.81	25.52	2796.29	7.06	3.74
2793.65	10.89	8.04	2794.53	6.82	4.97	2795.42	37.74	24.65	2796.30	7.72	4.15
2793.66	10.85	7.97	2794.54	5.59	7.39	2795.43	35.95	23.34	2796.31	7.67	4.50
2793.67	11.51	7.84	2794.56	5.89	8.74	2795.44	34.50	23.27	2796.32	7.56	4.00
2793.68	12.14	7.11	2794.57	6.11	7.04	2795.45	32.40	21.67	2796.34	6.69	4.84
2793.69	12.05	6.72	2794.58	7.06	5.80	2795.46	29.25	18.49	2796.35	6.46	6.67
2793.71	11.82	6.00	2794.59	8.05	5.81	2795.47	27.27	18.69	2796.36	6.74	5.44
2793.72	11.42	5.65	2794.60	8.35	5.74	2795.48	24.46	19.44	2796.37	6.32	3.90
2793.73	11.85	5.31	2794.61	8.48	5.50	2795.50	22.38	19.46	2796.38	6.98	3.05
2793.74	13.56	5.68	2794.62	8.19	5.55	2795.51	21.56	20.27	2796.39	6.68	3.58
2793.75	12.86	5.22	2794.63	7.08	5.79	2795.52	22.65	20.56	2796.40	7.10	4.61
2793.76	11.59	4.71	2794.65	6.98	5.46	2795.53	22.23	18.31	2796.41	7.47	5.34
2793.77	12.26	5.42	2794.66	8.78	5.23	2795.54	22.57	16.12	2796.43	7.17	5.05
2793.78	12.84	6.38	2794.67	9.26	4.75	2795.55	23.25	16.30	2796.44	7.44	4.53
2793.80	13.70	6.64	2794.68	8.35	4.32	2795.56	22.56	16.10	2796.45	6.12	3.96
2793.81	15.04	6.05	2794.69	5.90	3.71	2795.57	22.70	16.47	2796.46	6.53	3.97
2793.82	14.26	6.48	2794.70	5.31	2.79	2795.59	23.20	16.45	2796.47	6.69	3.22
2793.83	11.79	7.91	2794.71	5.68	2.48	2795.60	25.11	16.69	2796.48	11.55	3.54
2793.84	10.18	9.37	2794.72	6.92	2.89	2795.61	27.91	17.18	2796.49	11.19	3.75
2793.85	10.58	8.66	2794.74	7.48	2.98	2795.62	29.96	17.63	2796.50	9.51	2.83
2793.86	10.66	8.00	2794.75	6.60	3.32	2795.63	31.65	19.65	2796.51	7.93	4.44
2793.87	10.54	7.54	2794.76	5.85	3.67	2795.64	31.95	21.65	2796.53	9.23	4.81
2793.88	10.74	6.39	2794.77	4.38	3.37	2795.65	30.63	22.80	2796.54	9.72	4.65
2793.90	11.62	5.96	2794.78	3.21	1.98	2795.66	29.95	24.66	2796.55	8.96	4.52
2793.91	12.74	6.06	2794.79	3.09	1.44	2795.68	27.01	24.67	2796.56	9.08	4.67
2793.92	13.38	6.23	2794.80	3.30	1.56	2795.69	24.21	24.68	2796.57	9.79	4.93
2793.93	12.40	6.30	2794.81	4.93	1.93	2795.70	21.66	25.75	2796.58	9.88	4.74
2793.94	11.22	6.86	2794.82	2.59	2.38	2795.71	20.23	29.84	2796.59	9.63	5.85
2793.95	11.66	7.50	2794.84	3.26	2.18	2795.72	21.65	29.94	2796.60	9.43	5.22
2793.96	11.53	6.67	2794.85	4.16	1.23	2795.73	22.59	27.74	2796.62	9.34	6.41
2793.97	10.77	6.66	2794.86	4.40	1.17	2795.74	23.13	26.29	2796.63	9.77	6.18
2793.99	9.30	7.66	2794.87	4.53	1.86	2795.75	24.65	29.65	2796.64	9.12	6.28
2794.00	9.64	8.33	2794.88	5.37	2.33	2795.76	21.68	30.98	2796.65	9.31	5.86
2794.01	11.51	8.51	2794.89	5.65	2.60	2795.78	19.56	30.89	2796.66	9.43	4.93
2794.02	11.72	8.32	2794.90	5.26	3.14	2795.79	18.41	28.16	2796.67	9.08	4.93
2794.03	9.70	8.27	2794.91	6.01	2.94	2795.80	16.97	27.82	2796.68	8.86	6.00
2794.04	8.33	8.19	2794.93	7.00	3.10	2795.81	16.78	29.01	2796.69	8.23	7.01
2794.05	8.97	7.78	2794.94	6.46	3.08	2795.82	16.08	27.62	2796.70	8.46	6.43
2794.06	10.95	7.54	2794.95	6.41	3.56	2795.83	11.71	22.39	2796.72	9.23	5.77
2794.07	11.71	7.71	2794.96	7.05	5.02	2795.84	11.46	19.66	2796.73	9.42	6.68
2794.09	11.02	8.04	2794.97	6.66	5.98	2795.85	9.38	18.85	2796.74	9.22	7.81
2794.10	9.69	7.94	2794.98	5.23	5.44	2795.87	8.87	16.94	2796.75	8.85	7.72
2794.11	7.95	7.32	2794.99	4.82	4.09	2795.88	8.63	15.51	2796.76	9.87	6.57
2794.12	7.81	5.90	2795.00	4.98	3.43	2795.89	7.44	13.61	2796.77	11.25	5.72
2794.13	8.36	4.62	2795.01	4.70	4.23	2795.90	8.22	11.42	2796.78	10.41	5.08
2794.14	8.41	4.76	2795.03	5.07	7.25	2795.91	8.56	9.18	2796.79	9.57	4.89
2794.15	7.83	5.00	2795.04	5.22	9.32	2795.92	7.85	7.28	2796.81	9.75	5.23
2794.16	7.06	4.80	2795.05	5.40	7.17	2795.93	7.23	6.74	2796.82	10.58	5.68
2794.18	7.28	5.72	2795.06	5.77	5.42	2795.94	6.62	6.99	2796.83	11.48	5.11
2794.19	8.32	5.95	2795.07	5.32	5.35	2795.96	7.86	6.81	2796.84	11.02	5.11
2794.20	8.30	5.42	2795.08	5.75	4.83	2795.97	9.08	6.02	2796.85	10.51	5.15
2794.21	7.21	5.12	2795.09	6.81	5.61	2795.98	8.10	6.54	2796.86	10.23	5.39
2794.22	7.94	5.51	2795.10	7.29	6.44	2795.99	7.20	7.62	2796.87	9.21	5.04
2794.23	8.91	5.28	2795.12	7.17	7.72	2796.00	6.93	7.29	2796.88	8.56	4.68
2794.24	9.96	4.21	2795.13	7.65	8.15	2796.01	7.21	6.16	2796.90	9.65	3.95
2794.25	12.21	4.11	2795.14	8.82	8.68	2796.02	7.18	4.92	2796.91	10.44	4.50
2794.27	13.46	4.76	2795.15	9.51	9.18	2796.03	6.61	4.66	2796.92	10.86	5.71
2794.28	11.86	5.10	2795.16	9.17	9.55	2796.04	6.07	4.76	2796.93	11.94	6.12
2794.29	11.36	5.95	2795.17	8.85	10.63	2796.06	6.48	5.01	2796.94	11.90	6.52
2794.30	12.14	6.35	2795.18	9.40	13.10	2796.07	6.40	4.95	2796.95	11.17	5.78
2794.31	11.12	5.36	2795.19	10.76	16.52	2796.08	6.02	5.03	2796.96	11.19	5.54
2794.32	9.39	5.40	2795.21	12.79	17.77	2796.09	5.98	4.80	2796.97	11.47	6.45
2794.33	9.10	6.36	2795.22	15.84	16.54	2796.10	6.35	3.56			

■ $I(\lambda)$ units are ergs cm^{-2} s^{-1} sr^{-1} cm^{-1}

TABLE 1 (cont'd)

Absolute Spectral Intensities of MgII h and k

λ_{air} (Å)	$I(\lambda)\times10^{-12}$ ■ μ=1	$I(\lambda)\times10^{-12}$ μ=0.230	λ_{air} (Å)	$I(\lambda)\times10^{-12}$ ■ μ=1	$I(\lambda)\times10^{-12}$ μ=0.230	λ_{air} (Å)	$I(\lambda)\times10^{-12}$ ■ μ=1	$I(\lambda)\times10^{-12}$ μ=0.230	λ_{air} (Å)	$I(\lambda)\times10^{-12}$ ■ μ=1	$I(\lambda)\times10^{-12}$ μ=0.230
2800.91	12.23	6.80	2801.80	10.60	6.19	2802.68	22.12	13.94	2803.57	8.65	6.25
2800.92	12.45	6.78	2801.81	12.28	5.91	2802.69	21.41	14.64	2803.58	7.73	6.46
2800.94	12.53	6.76	2801.82	12.47	5.84	2802.70	20.79	14.39	2803.59	7.09	6.78
2800.94	12.45	6.76	2801.83	12.37	5.93	2802.72	20.31	13.92	2803.60	6.98	6.70
2800.95	12.45	6.76	2801.84	12.37	5.91	2802.73	20.65	14.61	2803.61	10.67	5.17
2800.96	12.99	6.91	2801.84	12.30	5.91	2802.73	19.97	14.64	2803.63	10.57	7.72
2800.97	13.46	6.93	2801.85	12.12	5.87	2802.74	19.98	13.33	2803.64	10.54	6.66
2800.98	14.14	6.72	2801.86	11.86	5.78	2802.75	18.47	14.64	2803.63	10.37	7.72
2800.99	13.68	6.66	2801.87	10.29	5.86	2802.76	19.99	16.33	2803.65	10.50	7.84
2801.00	12.93	6.52	2801.88	6.00	5.68	2802.77	20.60	15.47	2803.66	9.76	7.76
2801.01	11.19	6.72	2801.90	7.04	6.93	2802.78	21.04	13.70	2803.67	9.56	7.69
2801.03	8.72	6.60	2801.91	6.20	3.72	2802.79	22.35	13.80	2803.68	10.62	8.61
2801.04	7.24	7.71	2801.92	10.32	3.81	2802.81	23.02	14.42	2803.69	11.09	8.69
2801.05	6.35	6.74	2801.93	10.24	5.17	2802.82	24.14	15.15	2803.70	10.68	8.68
2801.06	5.08	3.74	2801.94	9.47	5.63	2802.83	24.42	17.81	2803.71	10.38	8.70
2801.07	3.86	3.38	2801.95	8.11	4.96	2802.84	24.01	17.84	2803.72	9.76	8.67
2801.08	3.39	3.08	2801.97	7.38	4.75	2802.85	27.13	17.99	2803.74	10.68	8.98
2801.09	3.84	2.72	2801.98	7.65	4.88	2802.86	30.48	19.28	2803.75	10.74	8.98
2801.10	5.62	2.75	2801.99	7.15	4.65	2802.87	33.36	21.18	2803.76	10.81	8.81
2801.11	6.81	3.64	2802.00	6.96	4.67	2802.89	32.51	23.58	2803.77	9.84	8.80
2801.13	13.07	4.05	2802.01	7.02	4.65	2802.90	28.26	25.87	2803.78	10.78	9.09
2801.14	15.58	3.84	2802.02	6.98	3.86	2802.91	27.10	27.93	2803.79	11.11	9.81
2801.15	15.53	3.82	2802.03	7.71	3.81	2802.92	29.65	30.27	2803.80	10.61	8.16
2801.16	14.23	3.67	2802.04	7.89	3.84	2802.93	33.31	30.82	2803.81	10.13	8.83
2801.17	12.96	4.43	2802.05	7.12	5.04	2802.94	35.56	29.55	2803.82	10.44	9.15
2801.18	11.20	5.73	2802.07	6.36	6.43	2802.95	37.12	32.83	2803.84	9.85	9.87
2801.19	10.66	6.54	2802.08	5.45	6.54	2802.96	32.24	35.98	2803.85	10.09	9.89
2801.21	12.48	7.91	2802.09	5.83	5.57	2802.97	27.31	41.83	2803.86	12.01	9.82
2801.22	14.68	8.72	2802.10	7.46	5.23	2802.99	24.87	41.21	2803.87	12.72	8.69
2801.23	14.61	7.99	2802.11	9.55	5.19	2803.00	23.37	39.61	2803.88	12.44	9.54
2801.24	13.24	6.93	2802.12	9.76	4.61	2803.01	22.58	37.72	2803.89	12.24	10.76
2801.25	13.07	6.60	2802.13	7.66	3.55	2803.02	21.61	37.04	2803.90	13.61	9.29
2801.26	12.36	5.33	2802.14	5.81	4.20	2803.03	19.98	34.11	2803.91	13.27	7.96
2801.27	10.36	5.82	2802.16	7.05	4.17	2803.04	18.04	32.40	2803.93	12.35	7.61
2801.28	10.66	7.44	2802.17	9.15	3.55	2803.05	16.05	29.04	2803.94	12.28	8.39
2801.30	12.36	8.75	2802.18	9.34	3.17	2803.06	14.59	31.14	2803.95	11.62	7.58
2801.31	12.95	8.42	2802.19	7.79	3.28	2803.07	13.44	28.74	2803.96	11.17	6.54
2801.32	13.27	8.57	2802.20	6.66	3.61	2803.09	12.40	26.98	2803.97	10.97	7.12
2801.33	13.11	9.18	2802.21	6.70	4.72	2803.10	11.61	24.91	2803.98	10.65	7.41
2801.34	12.81	9.26	2802.22	6.12	5.14	2803.11	11.23	24.51	2803.99	11.04	11.10
2801.35	13.65	10.02	2802.23	6.74	5.37	2803.12	10.53	24.38	2804.00	10.91	11.51
2801.36	14.46	11.57	2802.25	6.34	4.74	2803.13	10.04	24.26	2804.01	10.19	12.46
2801.37	14.31	11.53	2802.26	6.91	4.18	2803.14	9.23	24.93	2804.03	12.76	9.84
2801.38	13.58	10.44	2802.27	6.08	4.52	2803.15	8.92	24.34	2804.04	11.31	7.41
2801.40	12.74	9.23	2802.28	6.48	5.01	2803.16	8.05	24.50	2804.05	11.65	8.99
2801.41	12.60	8.04	2802.29	7.00	5.86	2803.18	7.30	24.69	2804.06	10.57	9.53
2801.42	14.15	6.77	2802.30	7.67	6.47	2803.19	7.01	24.73	2804.07	11.16	10.59
2801.43	14.12	6.03	2802.31	8.12	6.87	2803.20	6.91	3.61	2804.08	11.59	10.19
2801.44	12.63	6.11	2802.32	9.13	6.92	2803.21	6.79	3.22	2804.09	12.15	9.47
2801.45	10.94	6.08	2802.34	9.23	6.10	2803.22	7.01	3.13	2804.10	12.76	8.94
2801.46	11.50	6.50	2802.35	7.16	5.10	2803.23	6.86	3.04	2804.12	11.80	7.25
2801.47	12.56	6.34	2802.36	5.45	5.64	2803.24	7.16	2.71	2804.13	12.28	6.96
2801.48	12.08	6.25	2802.37	5.59	7.53	2803.25	7.10	2.58	2804.14	13.78	7.03
2801.50	12.05	7.41	2802.38	6.80	7.87	2803.26	6.61	3.20	2804.15	13.65	7.71
2801.51	11.77	8.81	2802.39	8.87	8.94	2803.28	6.81	3.91	2804.16	12.35	7.97
2801.52	12.02	8.54	2802.40	9.96	9.88	2803.29	7.05	3.99	2804.17	12.00	7.16
2801.53	12.97	5.57	2802.41	10.30	11.07	2803.30	7.77	4.67	2804.18	12.71	7.33
2801.54	13.07	4.74	2802.42	10.85	13.64	2803.31	8.84	5.95	2804.19	14.36	7.82
2801.55	11.81	5.56	2802.44	10.88	14.62	2803.32	8.52	5.84	2804.21	14.24	8.44
2801.56	11.03	7.54	2802.45	11.43	16.11	2803.33	8.40	5.46	2804.22	12.72	9.73
2801.57	10.70	7.48	2802.46	13.11	18.18	2803.34	8.60	6.02	2804.23	13.11	10.00
2801.59	10.80	6.82	2802.47	14.70	20.79	2803.?	7.16	6.69	2804.24	14.41	9.59
2801.60	11.10	6.51	2802.48	16.71	22.83	2803.3.	7.35	5.71	2804.25	14.59	9.64
2801.61	10.44	6.06	2802.49	18.95	23.31	2803.38	6.67	3.81	2804.26	15.42	8.85
2801.62	10.11	6.77	2802.50	21.36	23.71	2803.39	6.48	4.23	2804.27	14.45	7.64
2801.63	10.13	7.38	2802.51	24.05	25.77	2803.40	7.31	5.59	2804.28	14.50	7.33
2801.64	10.63	6.85	2802.53	27.08	28.33	2803.41	8.14	5.75	2804.30	13.55	7.61
2801.65	10.53	6.32	2802.54	28.03	30.05	2803.42	8.15	4.74	2804.31	14.37	7.34
2801.66	9.56	5.42	2802.55	27.81	30.24	2803.43	8.23	4.78	2804.32	13.63	7.13
2801.67	9.12	5.71	2802.56	26.47	28.52	2803.44	8.68	5.24	2804.33	13.30	7.69
2801.69	8.98	6.48	2802.57	24.81	26.80	2803.46	8.75	5.63	2804.34	14.53	8.55
2801.70	8.87	6.78	2802.58	24.89	25.48	2803.47	9.22	4.93	2804.35	14.51	9.61
2801.71	9.46	6.27	2802.59	40.75	22.83	2803.48	9.27	5.59	2804.36	12.61	10.02
2801.72	9.51	5.77	2802.60	38.22	19.11	2803.49	9.48	6.30	2804.37	12.44	9.73
2801.73	9.77	5.78	2802.62	36.76	17.11	2803.50	10.63	6.76	2804.38	14.36	9.03
2801.74	10.01	5.73	2802.63	35.05	16.89	2803.51	10.47	6.35	2804.40	15.59	9.33
2801.75	9.19	6.02	2802.64	30.45	16.46	2803.52	10.47	6.57	2804.41	15.35	10.18
2801.77	7.89	6.69	2802.65	26.87	16.50	2803.53	9.33	6.88	2804.42	14.39	10.60
2801.78	7.41	7.39	2802.66	26.30	15.14	2803.54	8.57	5.40	2804.43	15.18	10.00
2801.79	8.32	6.39	2802.67	24.50	13.63	2803.56	8.78	4.18			

■ $I(\lambda)$ units are ergs cm^{-2} s^{-1} sr^{-1} cm^{-1}

Table 3

Mg II h and k Inflection Points Data

Inflection Point	$\Delta\lambda$ (Å) $\mu = 1$	$I(\lambda)\times10^{-11}$* $\mu = 1$	$\Delta\lambda$ (Å) $\mu=0.23$	$I(\lambda)\times10^{-11}$ $\mu=0.23$
k_{1r}	+0.60	65	0.640	39.8
k_{2v}	-0.160	457	-0.190	360
k_{2r}	0.160	370	0.225	308
k_3	0.020	227	0.020	161
h_{1v}	-0.43	58.6	-0.50	41
h_{1r}	0.46	52.7	+0.50	36
h_{2v}	-0.120	408	-0.160	302
h_{2r}	0.160	334	0.220	279
h_3	0.040	200	0.030	133

*in ergs $cm^{-2}s^{-1}sr^{-1}cm^{-1}$

Table 4

Measured Parameters for Mg II h and k Emission Centers

Parameter	h $\mu = 0.230$ §	h $\mu = 1$ §	k $\mu = 0.230$ §	k $\mu = 1$ §	k $\mu = 1$ *
Separation of emission peaks (Å)	0.380	0.280	0.415	0.320	0.30
FWHM (Å)	0.60	0.48	0.680	0.530	0.56
Ratio between mean peak intensity and core intensity	2.18	1.86	2.07	1.82	2.2
Integral intensity $\times 10^{-5}$ (ergs $cm^{-2}s^{-1}sr^{-1}$)	1.48	1.72	2.04	2.24	
Ratio between core intensity and average minimum intensity	3.45	3.59	4.04	3.49†	2.38‡†
Ratio between average peak intensity and average minimum intensity				6.36	5.14‡†

*. Quiet sun reference profile (Lemaire and Skumanich 1973)
†. Using k_{1r} only
‡. Measured from Figure 3 (Lemaire and Skumanich 1973)
§. This work

Fig. 1 The observed solar spectrum near the Mg II h and k lines for "quiet regions" at $\mu = 1$ (upper) and $\mu = 0.23$ (lower).

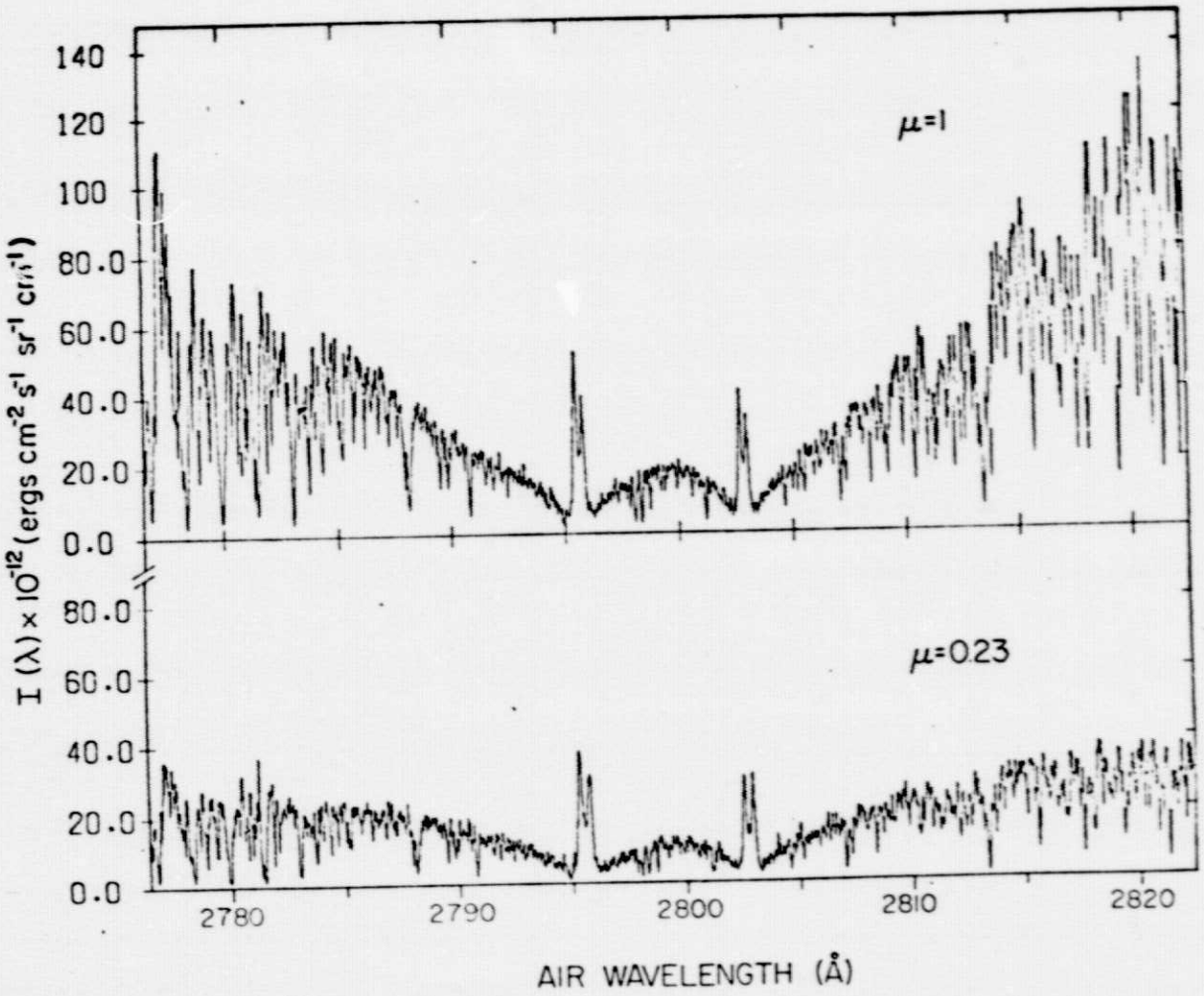
140
120
100
80.0
60.0
40.0
20.0
0.0
μ=1
80.0
60.0
40.0
20.0
0.0
μ=0.23
I (λ) × 10^-12 (ergs cm^-2 s^-1 sr^-1 cm^-1)
2780
2790
2800
2810
2820
AIR WAVELENGTH (Å)

Fig. 2 The emission centers of solar Mg II h and k. The raw data (triangles and crosses) are given for two scans at $\mu = 1$ (upper) and two scans at $\mu = 0.23$ (lower). The average data (solid line) for each set of scans after Fourier smoothing are also shown.

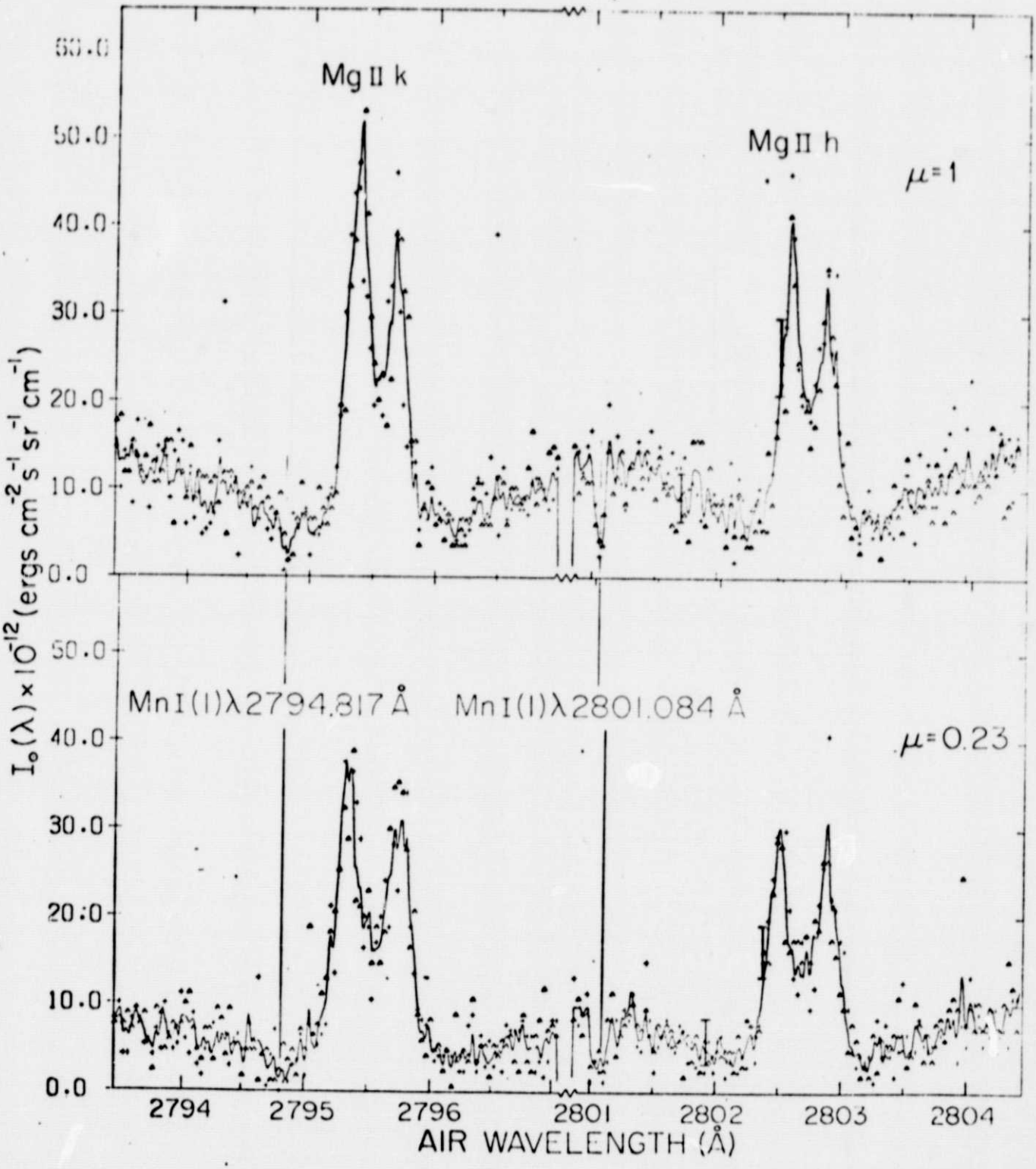
Mg II k
Mg II h
μ=1
Mn I (I) λ2794.817 Å
Mn I (I) λ2801.084 Å
μ=0.23
$I_o(\lambda) \times 10^{-12}$ (ergs cm^{-2} s^{-1} sr^{-1} cm^{-1})
60.0
50.0
40.0
30.0
20.0
10.0
0.0
50.0
40.0
30.0
20:0
10.0
0.0
2794
2795
2796
2801
2802
2803
2804
AIR WAVELENGTH (Å)

Fig. 3 A comparison of the emission center of Mg II h (dashed line) with Mg II k (solid line) for observations at $\mu = 1$ and at $\mu = 0.23$.

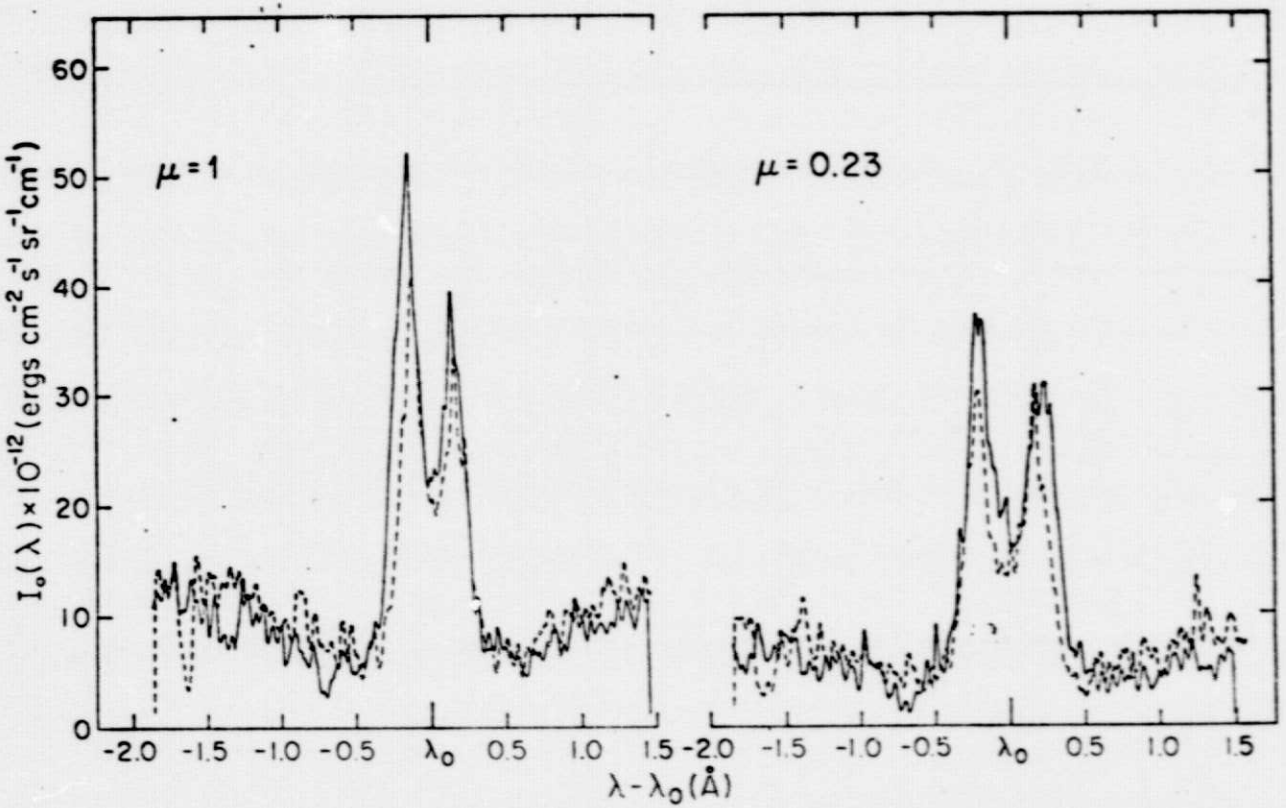
μ = 1
μ = 0.23
$I_o(\lambda) \times 10^{-12}$ (ergs cm^{-2} s^{-1} sr^{-1} cm^{-1})
0
10
20
30
40
50
60
-2.0
-1.5
-1.0
-0.5
λ_o
0.5
1.0
1.5
$\lambda - \lambda_o$ (Å)

Fig. 4 Representations of the Mg II h and k wings that were determined from regions of the spectrum that are apparently free of absorption lines.

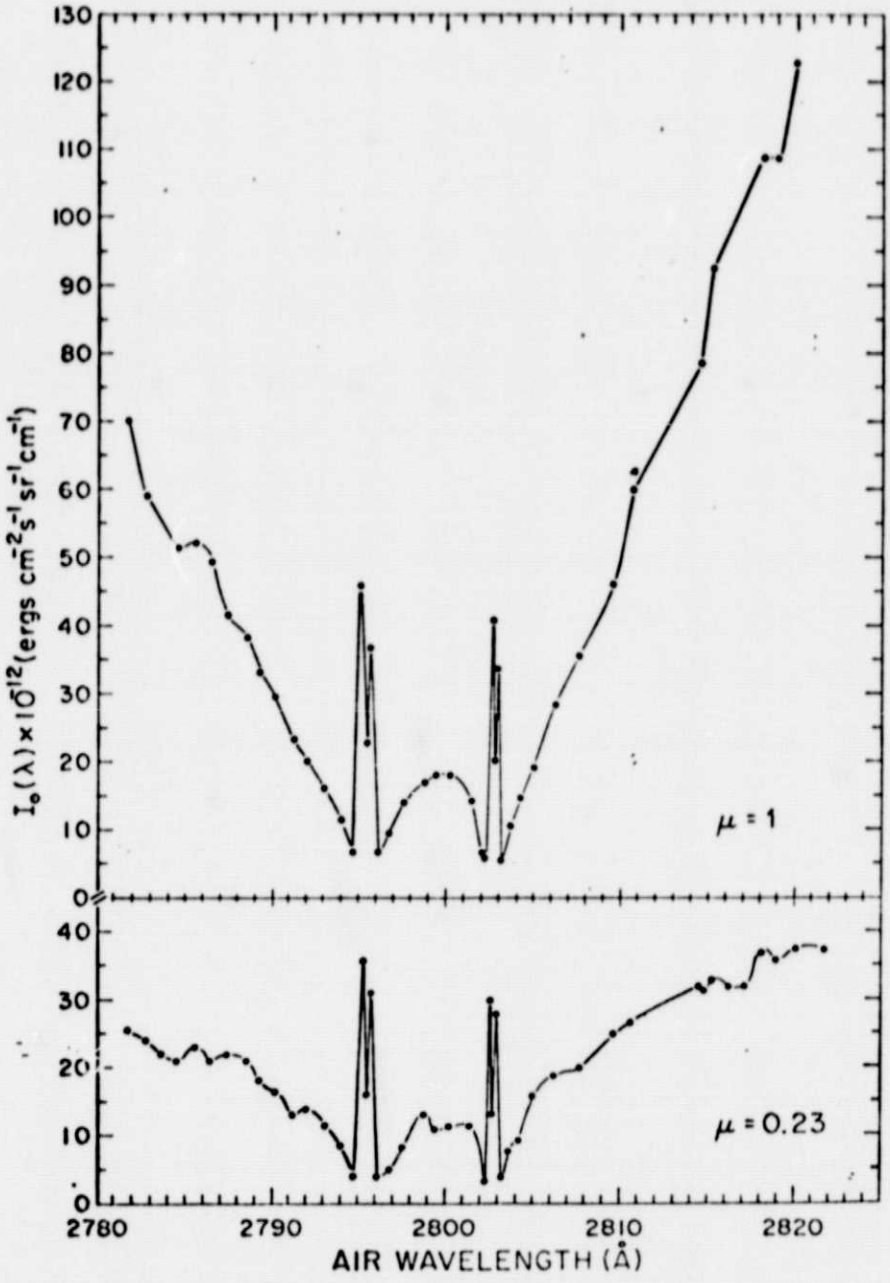
$I_o(\lambda) \times 10^{12}$ (ergs cm^{-2}s^{-1}sr^{-1}cm^{-1})
130
120
110
100
90
80
70
60
50
40
30
20
10
0
$\mu = 1$
40
30
20
10
0
$\mu = 0.23$
2780
2790
2800
2810
2820
AIR WAVELENGTH (Å)

Fig. 5 A plot of the ratio of the limb-to-center intensity ratio as a function of wavelength (μ = 1 to μ = 0.23).

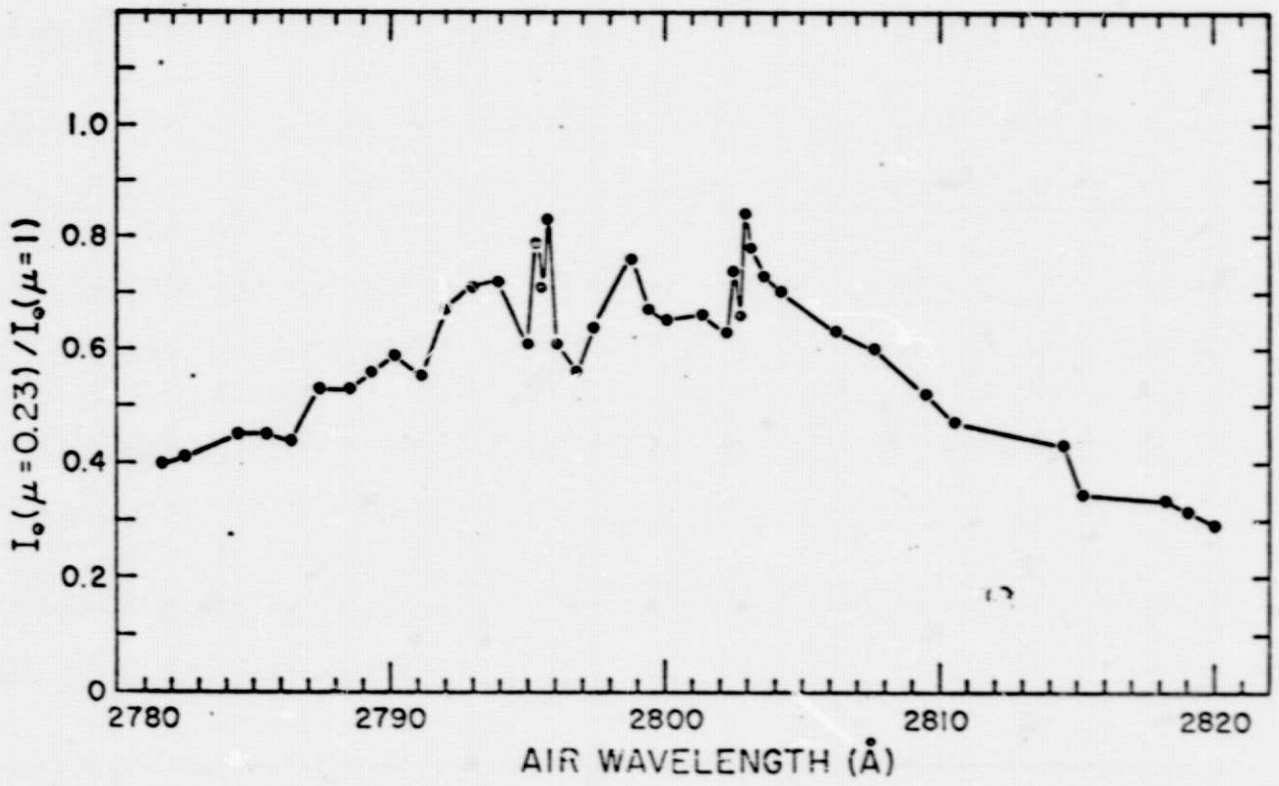
1.0
0.8
0.6
0.4
0.2
0
$I_o(\mu=0.23)/I_o(\mu=1)$
2780
2790
2800
2810
2820
AIR WAVELENGTH (Å)

Fig. 6 Raw data (+) and smoothed data (solid line) for measurements of the He II 1640 Å line.

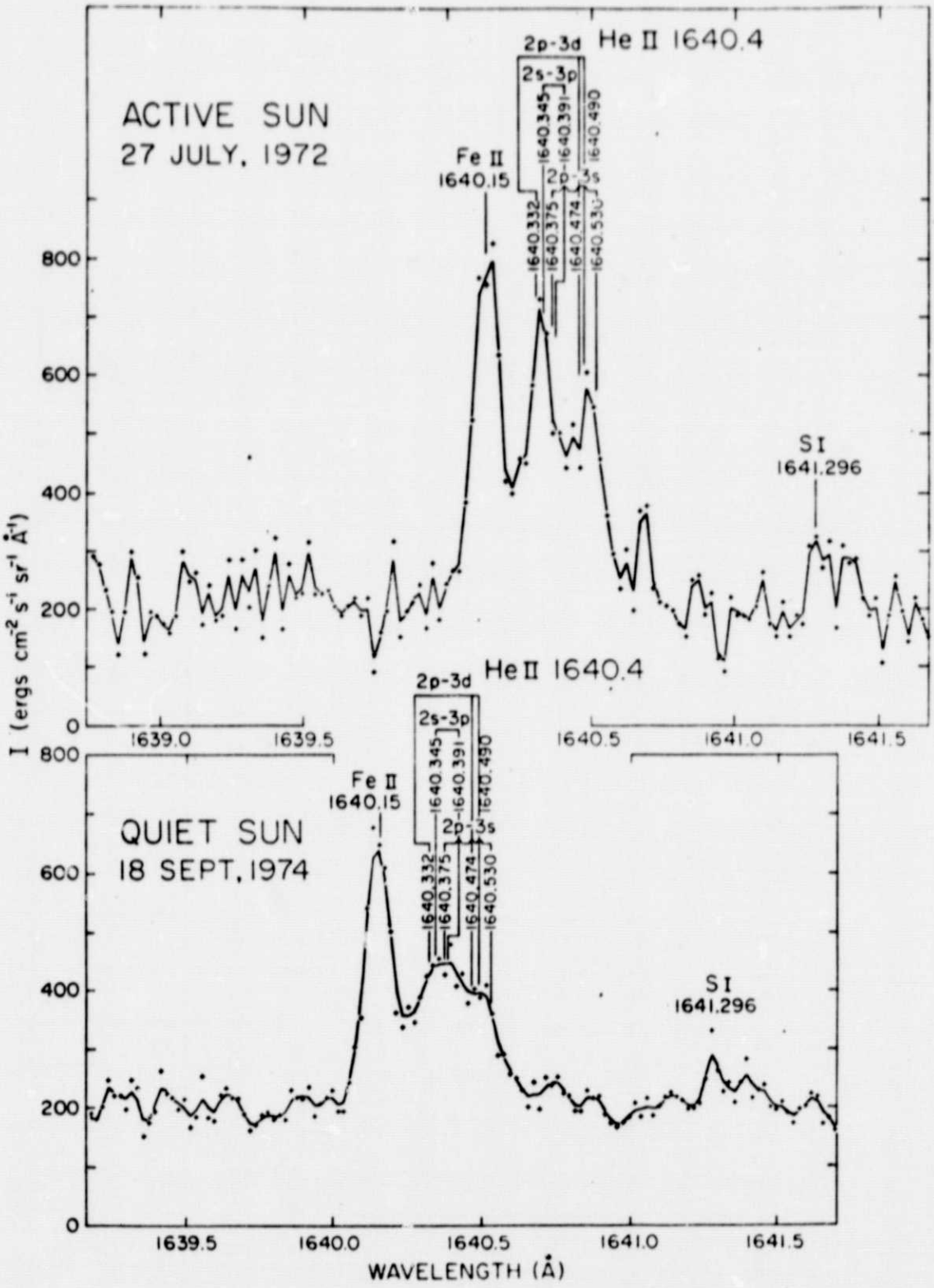
ACTIVE SUN
27 JULY, 1972
He II 1640.4
2p-3d
2s-3p
Fe II
1640.15
1640.345
1640.391
1640.490
1640.332
1640.375
1640.474
1640.530
SI
1641.296
QUIET SUN
18 SEPT, 1974
I (ergs cm⁻² s⁻¹ sr⁻¹ Å⁻¹)
WAVELENGTH (Å)
0
200
400
600
800
1639.0
1639.5
1640.0
1640.5
1641.0
1641.5

Fig. 7 Smoothed data (solid circles) and best fit curve (solid line) for observations of the He II 1640 Å line. The individual components of the He II line are also shown (solid line) in the lower part of the figure.

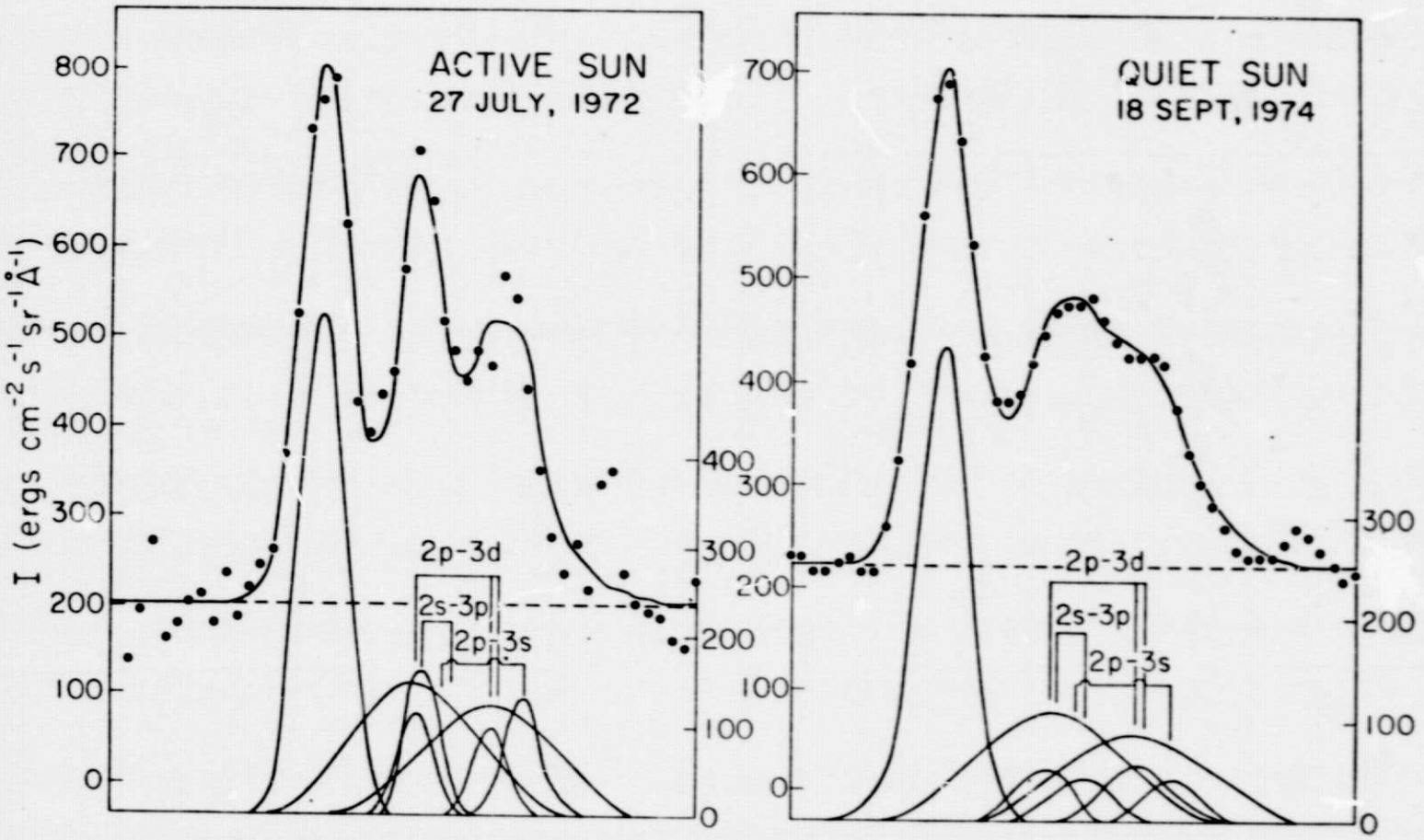
ACTIVE SUN
27 JULY, 1972
QUIET SUN
18 SEPT, 1974
I (ergs cm^{-2} s^{-1} sr^{-1} Å^{-1})
2p-3d
2s-3p
2p-3s
800
700
600
500
400
300
200
100
0

Fig 8. A plot of the system calibration function, $S(\lambda)$, against wavelength. Calibration points based on the calibration of our Spicer diode (open circles) are compared with points based on the calibration of a Philips standard lamp (solid circles).

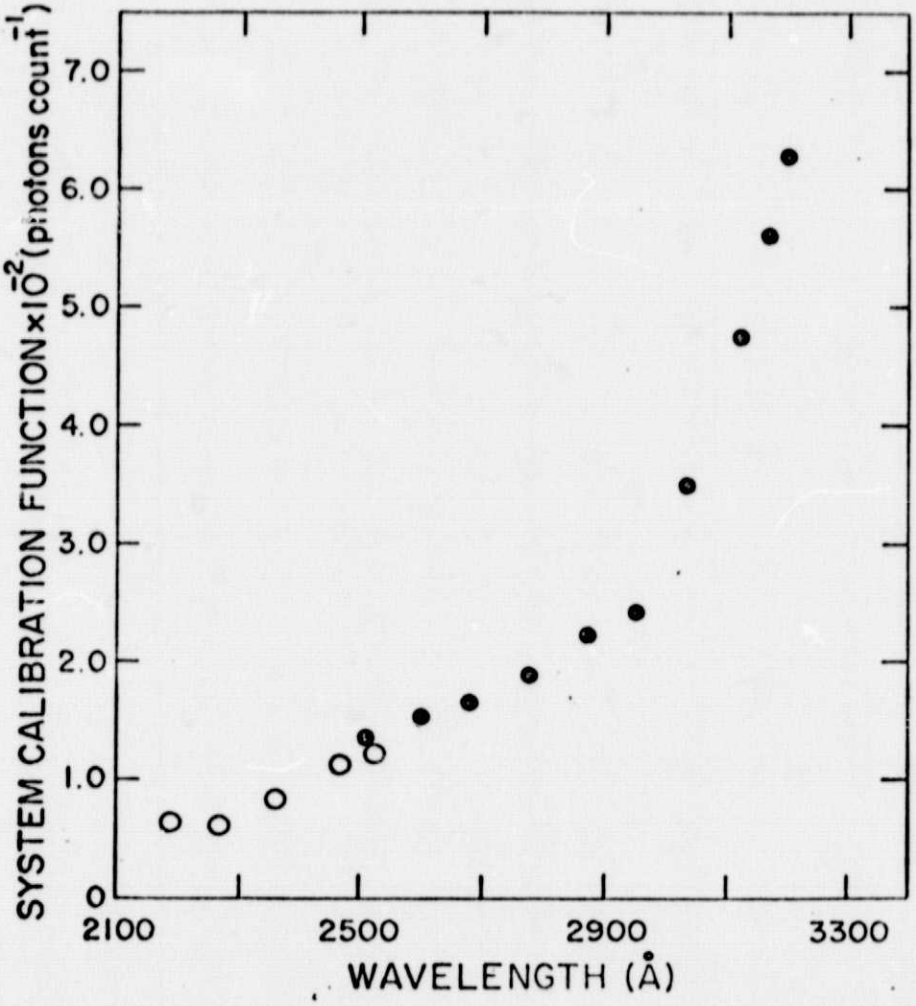
SYSTEM CALIBRATION FUNCTION×10^{-2}(photons count^{-1})
0
1.0
2.0
3.0
4.0
5.0
6.0
7.0
2100
2500
2900
3300
WAVELENGTH (Å)

Fig. 9 Lyman Alpha Scattered Light Test Facility.

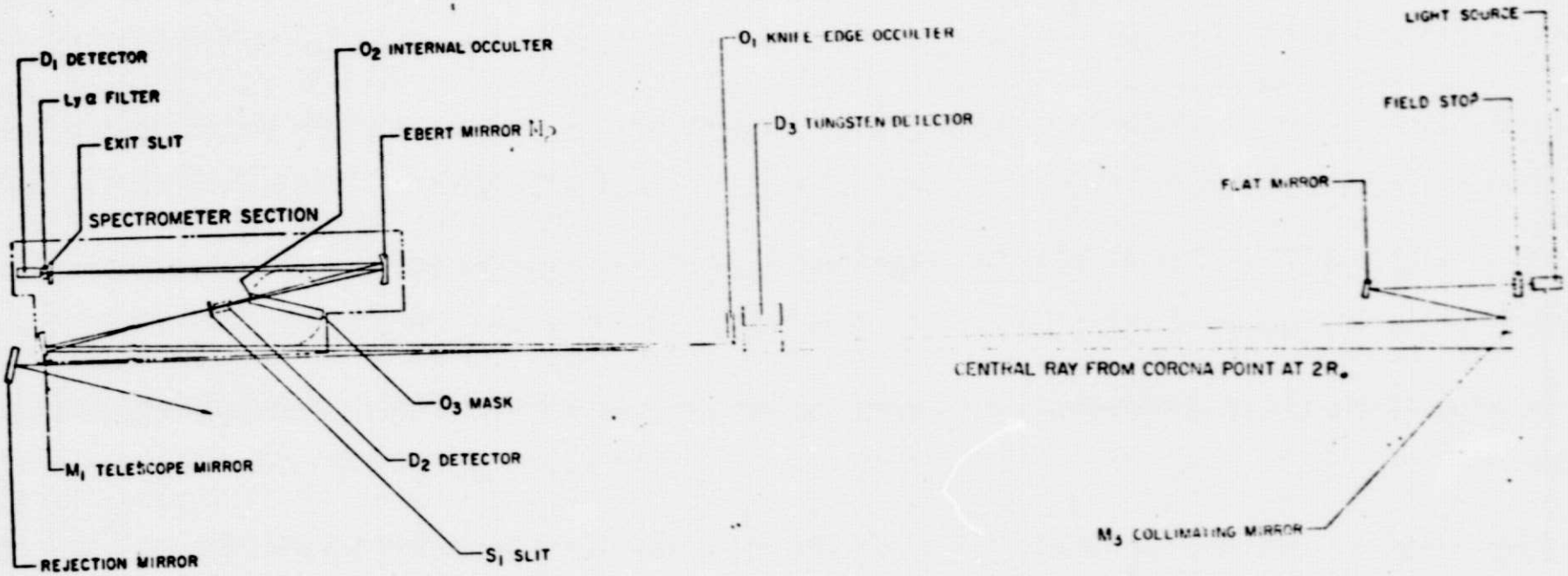

SCATTERED LIGHT TEST FACILITY

REFERENCES

Ayres, T.R., and Linsky, J.L., 1975, in press.

Cameron, A.G.W., Colgate, S.A., and Grossman, L., 1973, Nature, 243, 204.

De Vos, J.D., 1954, Physica, 20, 690.

Gabriel, A.H., and Jordan, C., 1972, Case Studies in Atomic Collision Physics, ed. McDaniel and McDowell, 2, North Holland Pub. Co. Amsterdam.

Grevesse, N., 1968, Solar Phys. 5, 159.

Hall, N.B., and Engvold, D., 1975, Ap. J. 197, 513.

Huber, M.C.E., and Parkinson, W.H., 1972, Ap. J., 172, 229.

Huber, M.C.E., Sandeman, J. and Tubbs, E., 1975, personal communication.

Kohl, J.L., 1974, IAU Colloquium 27, Cambridge, Mass., Sept.

Kohl, J.L., and Parkinson, W.H., 1974, Space Optics, (Washington, D.C. National Academy of Sciences), p. 511.

Kohl, J.L. and Parkinson, W.H., 1975a, Bull. AAS.

Kohl, J.L. and Parkinson, W.H., 1975b (submitted to Ap.J.).

Kohl, J.L., Parkinson, W.H., and Reeves, E.M. 1975, AAS Solar Phys. Div. Meeting, Boulder, Colorado, Jan.

Lemaire, P. 1971, Thesis, University of Paris.

Lemaire, P., and Skumanich, A., 1973, Astr. and Ap., 22, 61.

MacQueen, R.M., 1968, Applied Optics 7, 1149.

Milkey, R.W., and Mihalas, D., 1974, Ap.J., 192, 769.

Reeves, H., et al., 1970, Nature 226, 727.

Ryter, C., et al., 1970, Astron. and Ap., 8, 389.

Vernazza, J.E., Avrett, E.H., and Loeser, R., 1973, Ap. J. 184, 605.

Wohl, H., 1974, Astr. and Ap., 34, 41.